inter.noise 2014
MELBOURNE AUSTRALIA
16-19 NOVEMBER

Incorporating directivity in the Pseudospectral time-domain method by using spherical harmonics

Fotis GEORGIOU[1]; Maarten HORNIKX[2]

[1,2] Department of the Built Environment, Eindhoven University of Technology, Eindhoven, the Netherlands

ABSTRACT

A technique to incorporate directivity in the Pseudospectral time-domain method (PSTD) for auralization purposes is presented. The Pseudospectral time-domain method is a numerical method for solving the wave equation that requires only two spatial points per wavelength, making it more efficient compared to other wave based methods. The effect of source directivity as well as the head-related directivity have a clear influence on the perceived sound field and have to be included for the purpose of auralizations. In the less efficient finite difference time-domain method, directivity has been incorporated. Thus far, no such developments to incorporate directivity in PSTD have appeared. In this paper, directivity has been modeled by composing initial spatial distributions from spherical harmonic profiles and with the use of filters in order to achieve a frequency dependent directivity. The method is described in detail, drawbacks of the method and suggestions for further improvements are included.

Keywords: Pseudospectral time-domain method, source directivity, spherical harmonics, time-domain modeling

1. INTRODUCTION

The modeling of sound propagation has been achieved with various methods. The modeling methods can be separated into wave based methods and geometrical acoustic methods. The wave based methods are techniques used to solve the governing partial differential equation and the geometrical acoustics techniques consider sound waves as rays. Among the wave based methods are the finite difference time-domain method (FDTD), the pseudospectral time-domain method (PSTD), the boundary and finite element method (BEM, FEM), the digital waveguide mesh (DWM), the equivalent source method (ESM), the functional transformation method (FTM) and the parabolic equation (PE). Popular geometrical acoustics methods are the ray-tracing and the image source method (ISM).

The head-related directivity and source directivity play a very important role in the perception of an acoustic field. By incorporating directivity in auralization the quality of the simulation is significantly improved (1). Previously, source directivity has been modeled with wave based methods such as FDTD (2, 3, 6, 7, 8, 9, 10), DWM (4, 5) and ESM (9, 10), as well as with geometrical acoustics methods (1, 11). The main goal of this work is to implement source directivity in the PSTD method, which is something that has not been implemented yet.

Some techniques to incorporate source directivity with potential applicability in PSTD have been previously developed. Escolano et al. (2) modeled directional sources based on directivity diagrams for discrete frequencies. Arrays of monopoles were used to create a particular sound field based on directivity diagrams taken from literature. The driving function of each source had an associated amplitude weight and a phase delay. The weights were calculated using a Least-squares method allowing the creation of several directivities for different discrete frequencies in a single simulation. One of the advantages of this method is that since it makes use of monopoles, it can easily be implemented in any discrete-space method (results from the analysis showed that the directivity diagrams produced with this method are the same for the FDTD, DWG and FTM). The main disadvantages of this technique are that the sound field resolution depends on the point source distribution therefore it is possible to synthesize a limited bandwidth only for a given source distribution, and moreover the method is not valid for the near field. In a more recent paper, Escolano et al. (3) proposed an extension of their previous method to incorporate broadband directive sources with a frequency-dependent

[1] f.georgiou@tue.nl
[2] M.C.J.Hornikx@tue.nl

directivity. Vecherin et al. (9) incorporated source directivity into outdoor sound propagation calculations using the ESM and the directional starter method (DSM). Both of these methods are frequency-domain techniques, but Wilson et. al (10) state that ESM has the potential to be applicable for time-domain methods. Vecherin et al. are looking for compact source distributions that produce a given directivity function in the far field using the ESM technique (9). Their goal is to find as few point sources as possible to produce a specified directivity function. The method can be separated into three steps: 1) decompose the directivity function into spherical harmonics, 2) relate each spherical harmonic to an elementary source configuration, 3) the final source distribution that produces a given directivity function will be a linear combination of the elementary configurations. A main advantage of this method is that the source configuration is compact, which is not the case in the method developed by Escolano et al.. Southern and Murphy (8) proposed a method for the implementation of first order directional source patterns (cardioid, sub-cardioid etc.) using two closely spaced monopole sources with opposite polarity and with the radiation pattern varied by changing a delay variable and the weighting of the omnidirectional and directional components. Overall, this method provides a good alternative to a more complex implementation of source directivity for approximating first order directional patterns. An additional advantage of this method is that provides a more accurate near field response compared to Escolano's method. Sakamoto et al. (6, 7) models sound radiation characteristics from a mouth simulator in FDTD using different directional source components with spherical harmonic profiles. The technique used in this work is based on the method developed by Sakamoto et.al. and it is described in detail in section 3.

This paper is organized as follows. The Fourier PSTD method with Runge-Kutta time-stepping scheme is described in section 2. Section 3 deals with 1) the decomposition of a directivity function using spherical harmonics and 2) the method designed to compose a directivity function in PSTD using initial distributions with spherical harmonic profiles. A computational example is given in section 4. Finally, in section 5 conclusions and method's drawbacks are presented.

2. PSEUDOSPECTRAL TIME-DOMAIN METHOD

2.1 Introduction to PSTD

The pseudospectral (PS) method is used to calculate the spatial derivative operator of a time-dependent problem (12). The time-marching scheme is operated by another method and their combination is referred to as PSTD. The most popular PS methods are the Fourier PS and the Chebyshev PS methods. In this work, the Fourier PS method was used. Fourier PS assumes that the spatial domain is periodic and the spatial derivatives are estimated in the wave number domain using Fourier transforms (13). In PS methods the computation of the spatial derivative at a discrete point depends on the values of all points in the domain, whereas in the finite difference (FD) methods the computation depends only on the neighboring points. Therefore, the PS methods are referred to as global methods and FD as local methods. In Equation (1) is demonstrated how the one dimensional linear wave equations are transformed by the Fourier PS:

$$\begin{aligned} \frac{\partial u}{\partial t} &= -\frac{1}{\rho_0}\mathscr{F}_x^{-1}\left(jk_x\mathscr{F}_x^1(p)\right) \\ \frac{\partial p}{\partial t} &= -K\mathscr{F}_x^{-1}\left(jk_x\mathscr{F}_x^1(u)\right) \end{aligned} \tag{1}$$

with u the acoustic velocity perturbations, p the acoustic pressure perturbations, $\mathscr{F}^1, \mathscr{F}^{-1}$ the forward and inverse Fourier transform over and to the direction of x, k_x the wave number for the x-direction, ρ_0 the air density and K the bulk modulus. Due to the Nyquist theorem, only two spatial points per wavelength are required to obtain high-accurate results. This makes PSTD more computational efficient than other wave based methods (12, 14, 15).

2.2 Runge-Kutta scheme

The Runge-Kutta methods are low-dissipation and low-dispersion time-stepping schemes (12, 14, 16). Runge-Kutta methods compute a single discrete time step by several intermediate steps, thereby they achieve a higher order accuracy compared to the second-order accurate finite differences scheme (12, 16). The time derivative operator of Equation (1) is here calculated with a low storage optimized six-stage Runge-Kutta method developed by Bogey and Bailly (16). The method has optimized the dispersion and dissipation errors for frequencies corresponding up to four points per wavelength. Equation (1) for the acoustic pressure can be

solved by the Runge-Kutta method as:

$$\begin{aligned} &p(x,t_0) = p(x,t) \\ &p(x,t_i) = p(x,t_0) - \gamma_i \Delta t K \mathscr{F}_x^{-1}\left(jk_x \mathscr{F}_x^1(u_x)\right) \\ &\text{for} \quad i = 1...6 \\ &p(x,t+\Delta t) = p(x,t_6) \end{aligned} \tag{2}$$

with i the integer stage number within the Runge Kutta time step, $\gamma_i \in [0,1]$ the Runge-Kutta coefficients as given in (16).

3. MODELING SOURCE DIRECTIVITY

3.1 Spherical harmonics

Spherical harmonic (SH) functions are a hierarchical set of basis functions which are orthogonal upon a surface of a sphere (17). Any directivity function $d(\theta,\phi)$ can be expressed as an infinite summation of series of SH functions as in Equation (3).

$$\begin{aligned} d(\theta,\phi) &= \sum_{n=0}^{\infty} \sum_{m=-n}^{n} A_n^m Y_n^m(\theta,\phi) \\ Y_n^m(\theta,\phi) &= \sqrt{\frac{2n+1}{4\pi}\frac{(n-m)!}{(n+m)!}} P_n^m(\cos\theta) e^{jm\phi} \end{aligned} \tag{3}$$

with ϕ the azimuth ($0 \leq \phi \leq 2\pi$), θ the elevation ($0 \leq \theta \leq \pi$), Y_n^m the SH functions of degree n and order m, P_n^m the associated Legendre polynomials, and A_n^m the SH expansion coefficients. The SH functions are complex and need to be converted into real functions in order to be appropriate for PSTD analysis (7):

$$\begin{aligned} X_n^m &= \frac{1}{2}(Y_n^{-m} + (-1)^m Y_n^m) \quad &\text{if m>0} \\ X_n^m &= Y_l^m \quad &\text{if m=0} \\ X_n^m &= \frac{1}{2} j(Y_n^{-m} - (-1)^m Y_n^m) \quad &\text{if m<0} \end{aligned} \tag{4}$$

with X_n^m the real type SH functions of degree n and order m. In practice the outer summation of Equation (3) is truncated to a degree l:

$$d(\theta,\phi) = \sum_{n=0}^{l} \sum_{m=-n}^{n} C_n^m X_n^m(\theta,\phi) \tag{5}$$

with C_n^m the real type SH expansion coefficients.

3.2 Spherical harmonic decomposition

Before composing any directivity function $d(\theta,\phi)$ in PSTD, it first has to be decomposed. The locations that constitute the directivity function will be referred as directivity grid. The decomposition can be done with three methods, the direct integration method, the Least-squares (LS) method, and the regularized LS method (18). The LS method has here been used because as is stated in reference (18) it works better for arbitrary grid as opposed to the direct integration method which requires specific quadrature points and fails if an arbitrary grid is used.

The decomposition is implemented in the frequency domain. Assume that the directivity function $d(v,F)$ (with v the continuous vector of the directivity locations and F the frequency response of each of the locations) consists of L locations and the frequency response F is N samples long. The decomposition is now done for every frequency component of F separately. In matrix notation it is written as:

$$D = \begin{pmatrix} d(v_1,F_1) & d(v_1,F_2) & \cdots & d(v_1,F_N) \\ d(v_2,F_1) & d(v_2,F_2) & \cdots & d(v_2,F_N) \\ \vdots & \vdots & \ddots & \vdots \\ d(v_L,F_1) & d_L(v_L,F_2) & \cdots & d(v_L,F_N) \end{pmatrix} \tag{6}$$

The real type SH functions truncated at degree l in matrix notation is $L \times (l+1)^2$:

$$X = \begin{pmatrix} X_0^0(v_1) & X_1^{-1}(v_1) & X_1^0(v_1) & X_1^1(v_1) & \cdots & X_l^l(v_1) \\ X_0^0(v_2) & X_1^{-1}(v_2) & X_1^0(v_2) & X_1^1(v_2) & \cdots & X_l^l(v_2) \\ \vdots & \vdots & \vdots & \vdots & \ddots & \vdots \\ X_0^0(v_L) & X_1^{-1}(v_L) & X_1^0(v_L) & X_1^1(v_L) & \cdots & X_l^l(v_L) \end{pmatrix} \tag{7}$$

Equation (5) for the q^{th} frequency component in matrix notation is written as:

$$D_{*,q} = C_{*,q}X \tag{8}$$

where $D_{*,q}$ is the q^{th} column of D matrix and $C_{*,q}$ the q^{th} column of C matrix (Equation (9)). Equation (8) can be solved with the LS method which can be implemented in MATLAB using the backslash command (19). The C matrix that contains the SH expansion coefficients of the directivity function in the frequency domain is a $(l+1)^2 \times N$ matrix:

$$C = \begin{pmatrix} C_0^0(F_1) & C_0^0(F_2) & \cdots & C_0^0(F_N) \\ C_1^{-1}(F_1) & C_1^{-1}(F_2) & \cdots & C_1^{-1}(F_N) \\ C_1^0(F_1) & C_1^0(F_2) & \cdots & C_1^0(F_N) \\ C_1^1(F_1) & C_1^1(F_2) & \cdots & C_1^1(F_N) \\ \vdots & \vdots & \ddots & \vdots \\ C_l^l(F_1) & C_l^l(F_2) & \cdots & C_l^l(F_N) \end{pmatrix} \tag{9}$$

3.3 Directivity composition

The first step of the directivity composition in PSTD is to obtain initial conditions with SH profiles which will be used as basis functions to compose the desirable directivity. Sakamoto et.al (6, 7) describe thoroughly how real-type SH functions can be obtained by a combination of higher order spatial derivatives of the pressure distribution. By choosing an omnidirectional Gaussian pressure distribution as initial condition (Equation (10))

$$p(r,t_0) = e^{-\frac{r^2}{w^2}} \tag{10}$$

where $r = \sqrt{(x-x_s)^2+(y-y_s)^2+(z-z_s)^2}$, (x,y,z) are the Cartesian coordinates, (x_s,y_s,z_s) the coordinates of the distribution's center and $w = \Delta_x/\sqrt{0.3}$ determines the width of the Gaussian signal which can be regarded as being band limited up to $f_s/2$ with fs the spatial sampling frequency and Δ_x the spatial step (12). Then, the initial conditions with SH profile obtained by the linear combination of the spatial derivatives of p are listed in Table 1 (7).

Table 1 – Spatial distributions with SH profiles.

Degree n:	Initial distribution	Order m:
$n=0$	$pX_0^m = e^{-\frac{r^2}{w^2}}X_0^0$	$m=0$
$n=1$	$\frac{\partial p}{\partial r}X_n^m = -\frac{2r}{w^2}e^{-\frac{r^2}{w^2}}X_n^m$	$m=(-1,0,1)$
$n=2$	$\frac{\partial^2 p}{\partial r^2}X_n^m = \frac{4r^2}{w^4}e^{-\frac{r^2}{w^2}}X_n^m$	$m=(-2,-1,0,1,2)$
$\vdots$	$\vdots$	$\vdots$
$n=l$	$\frac{\partial^l p}{\partial r^l}X_n^l = \cdots$	$m=(-l,\cdots,l)$

Figure 1 shows the spatial distributions, transient, and frequency response of the initial distributions of degree n=0 and order m=0 [0,0] and degree n=2 and order m=1 [2,0] of Table 1. The frequency responses of the two initial distributions are different as it is demonstrated in Figure 1. When composing a directivity function from a combination of initial distributions with SH profiles it is desirable that all the initial distributions have identical responses. In order to achieve that, inverse filters have been designed. The transient response of the spatial distribution [0,0] was used as a target response and the goal was to design inverse filters that will make all the responses of the spatial distributions identical to the target response.

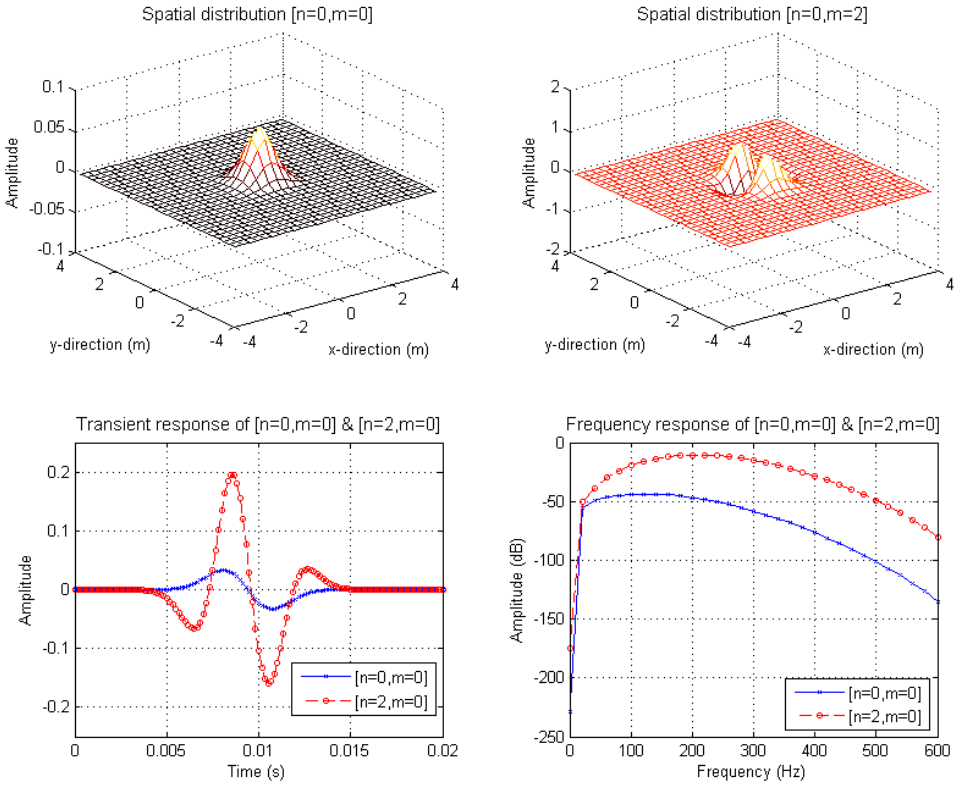

Figure 1 – Plots of spatial distributions of initial conditions in 2D with their transient and frequency responses recorded at 3 meters from the center of the spatial distributions.

LS deconvolution with frequency-independent regularization was used to design the inverse filters (20, 21). The LS deconvolution minimizes the error between the target response and the response of the other spatial distribution. The frequency-independent regularization is employed to attenuate the high frequency components of the inverse filter by choosing an appropriate weighting factor. Assuming that f_0 is the target response (in time domain) and f_2 the transient response of the initial distribution [2,0] then the inverse filter Inv_2 is calculated by the following expression:

$$Inv_2 = [\mathbf{F_2^T F_2} + \beta \mathbf{I}]^{-1} \cdot \mathbf{F_2^T} f_1 \tag{11}$$

with $\mathbf{F_2}$ the convolution matrix of f_2, $\mathbf{I}$ the identity matrix and β the regularization weighting factor which is a scalar $\in [0, 1]$. The weighting factor was chosen such that the difference of the frequency response between f_0 and f_2 is minimal for the frequencies bellow $fs/2$.

High frequency component artifacts (low amplitude ripples in the response of the inverse filter) occurred due to the LS deconvolution. To minimize this effect a low-pass filter (LPF) with cut-off frequency at $fs/2$ was applied to the inverse filter. The response of the inverse filter computed with Equation (11) and after the low-pass filtering is shown in Figure 2. The result of the convolution of f_2 with Inv_2 is demonstrated in Figure 3. A flow chart of the method is presented in Figure 4.

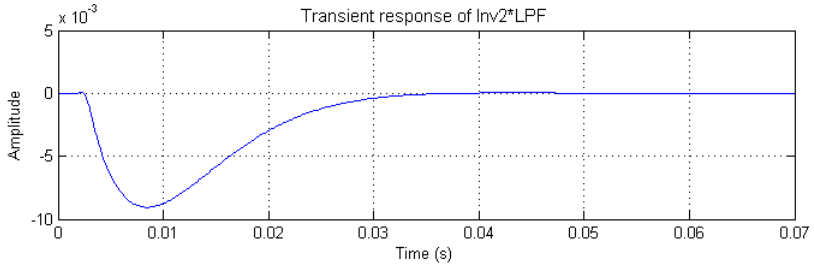

Figure 2 – Transient response of the inverse filter of degree 2 convolved with the low-pass filter

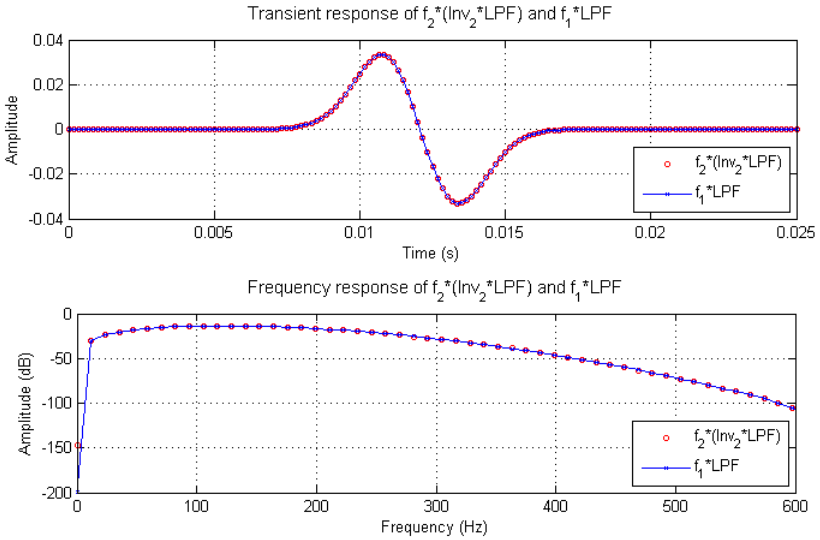

Figure 3 – Effect of Inverse filter Inv_2 when applied to f_2

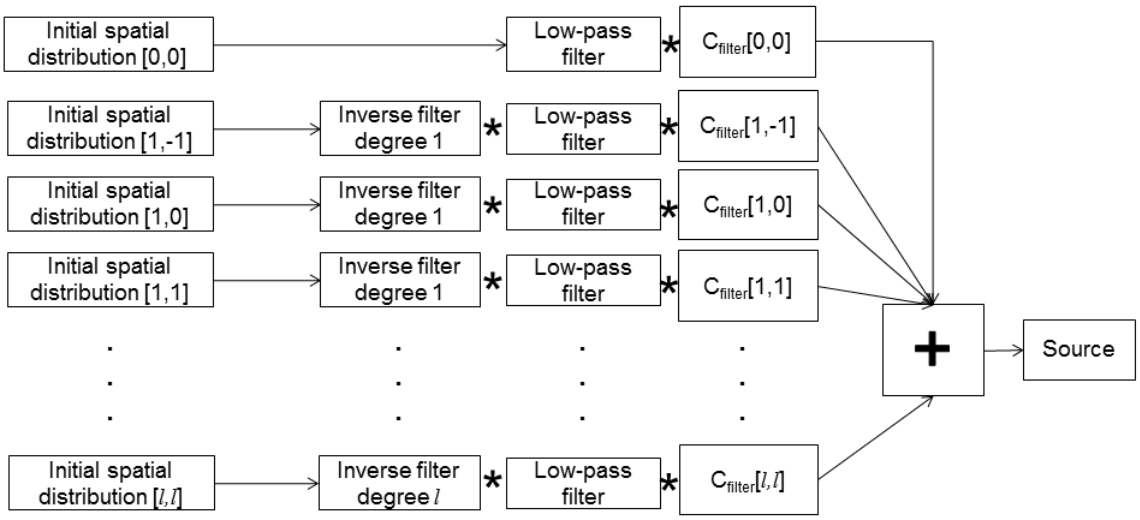

Figure 4 – Method flowchart

The initial distributions of the same degree have the same frequency response. Therefore, the same inverse filter is used for the initial distributions of the same degree. The C_{filter} are FIR filters which are computed with inverse Fourier transform (IFT) of the rows of C matrix in Equation (9), e.g. the $C_{filter}[0,0]$ is the IFT of the first row of C. The convolution of the inverse filters with the low-pass filter and with the C_{filter} is done prior the simulation in order to multiply the resulting filters with the initial spatial distributions inside the update equation (Equation (2)). These filters will be called $filt_{n,m}$ e.g. the resulting filter from the convolution of the *inverse filter order 1* with the *Low-pass filter* and the $C_{filter}[1,1]$ will be referred to as $filt_{1,1}$. Since the multiplication between the *Initial spatial distribution [n,m]* with the corresponding $filt_{n,m}$ takes place during the equation update with a Runge-Kutta time stage, all the $filt_{n,m}$ need to be resampled at Runge-Kutta time steps. The Runge-Kutta time steps are non-integer numbers therefore the resampling has to take place in the frequency domain by multiplying the frequency response of $filt_{n,m}$ with $e^{j\omega\Delta t\cdot\gamma(i)}$ as in the following equation:

$$filt_{nm}(i,:) = \mathscr{F}^{-1}\left(e^{j\omega\Delta t\cdot\gamma(i)}\mathscr{F}(filt_{n,m})\right) \quad \text{for} \quad i = 1\ldots6 \tag{12}$$

with ω the angular frequency and Δt the discrete time step.

The method used to insert the *Initial spatial distribution [n,m]* with the corresponding $filt_{n,m}$ in the update equation is demonstrated in the next equation:

$$\begin{aligned} &p(x,t_0) = p(x,t) \\ &p(x,t_i) = p(x,t_0) + \gamma_i \Delta t \left(-K\mathscr{F}_x^{-1}\left(jk_x \mathscr{F}_x^1(u_x)\right) + ISD[0,0]\cdot filt_{0,0}(q) + ISD[1,-1]\cdot filt_{1,-1}(q)\cdots\right) \\ &\qquad q = q+1 \\ &\text{for} \quad i = 1...6 \\ &p(x,t+\Delta t) = p(x,t_6) \end{aligned} \tag{13}$$

with q the index of the time step and ISD the initial spatial distribution.

4. COMPUTATIONAL EXAMPLE

The modeling method described in the previous section was applied to a calculation of the directivity characteristics from a dipole source. The dipole source was modeled analytically with the same directivity characteristics at all frequencies. The dipole source was band limited up to 600Hz which is equivalent to the Nyquist spatial sampling frequency used in the PSTD simulation ($fs/2 = 600$Hz). The impulse and frequency response of the dipole source at 90° azimuth and 0° elevation is shown in Figure 5. The transient response of $C_{filter}[1,-1]$ obtained by the SH decomposition of the dipole source is demonstrated in Figure 6. In the PSTD simulation the spatial discretization was set to $\Delta_x = c/fs$ and the time step $\Delta_t = \Delta_x/(5c)$, with $c = 343m/s$ the speed of sound. Comparison between the original dipole directivity and the modeled dipole directivity at 0° elevation in three different octave bands is shown in Figure 7. The differences between the directivity pattern of the modeled and original dipole are almost negligible.

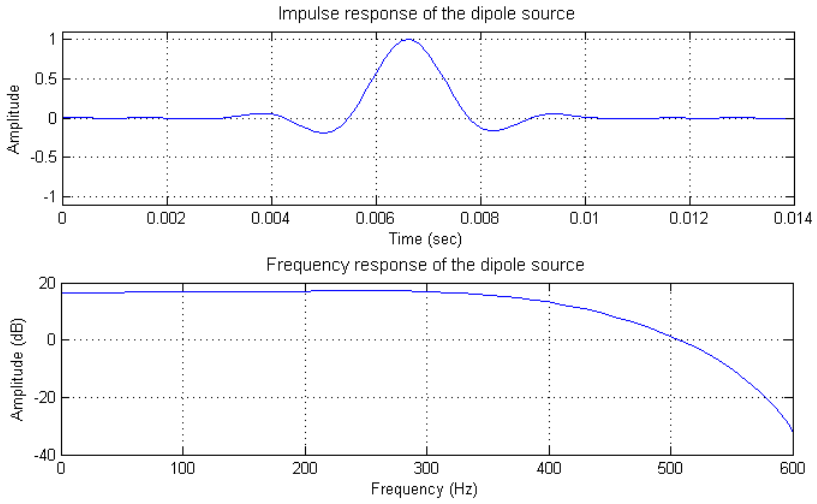

Figure 5 – Impulse and frequency response of the dipole source at 90° azimuth and 0° elevation

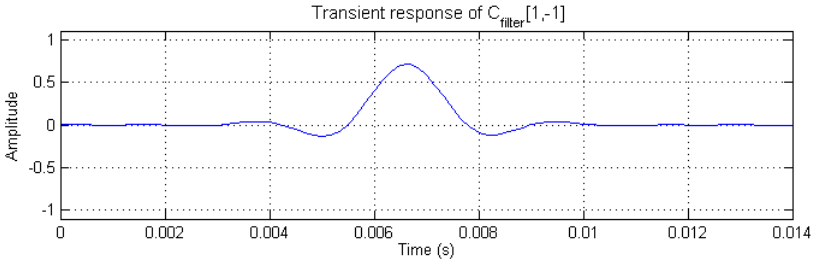

Figure 6 – Transient response of $C_{filter}[1,-1]$ obtained by the SH decomposition of the dipole source

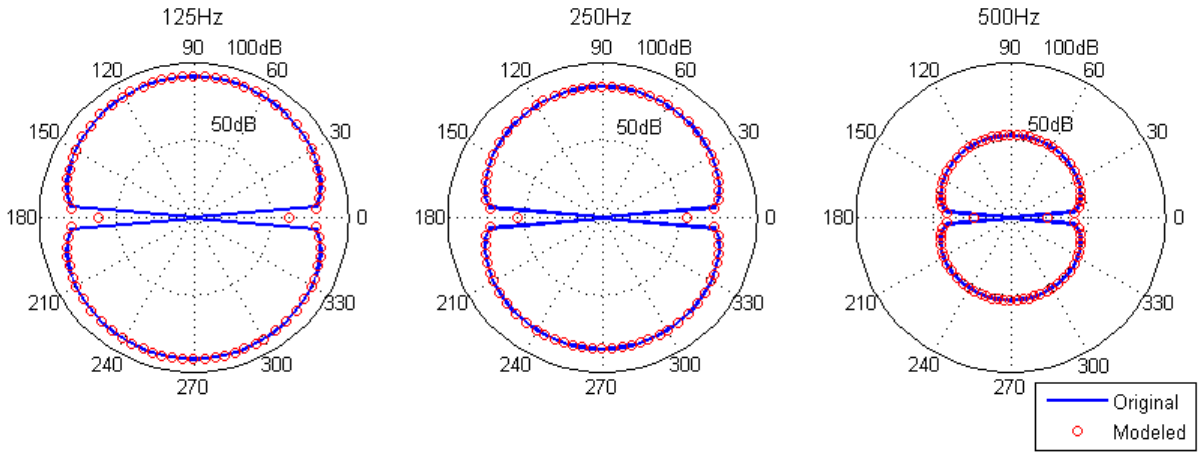

Figure 7 – Original vs Modeled dipole directivity at 3 different octave bands

5. FINAL REMARKS

An approach to incorporate directivity in PSTD by using initial distributions with SH profiles, was described in this paper. By decomposing a directivity function with real type SH functions, then this directivity can be composed in PSTD with the combination of spatial distributions with SH profiles together with digital filters. It was shown that this approach yields to accurate results for a dipole directivity. More results of sources with more complex directivity are coming.

The main drawback of this method is the low computational efficiency if many initial spatial distributions are used to compose the source directivity. The $filt_{n,m}$ are multiplied with the 3D *Initial spatial distribution [n,m]* during the equation update with the Runge-Kutta time step (Equation (13)). The length of the $filt_{n,m}$ depends on the size of the *Inverse filter degree n* and the $C_{filter}[n,m]$ which are convolved together to form the $filt_{n,m}$. The length of the $filt_{n,m}$ is large and this is mainly caused from the size of the *Inverse filter degree n* that is computed with the LS deconvolution (Equation (11)). As it can also be seen in the work from Sakamoto et al. (7), the length of the inverse filters is twice the length of the transient response of the initial spatial distributions. Assuming that the length of the $filt_{n,m}$ is N samples long (resampled at Runge-Kutta time steps) the multiplication between the $filt_{n,m}$ and the corresponding *Initial spatial distribution [n,m]* has to take place N times during the update equation (Equation (13)). A good improvement for the method would be to develop a technique to design shorter inverse filters. Another drawback of the method is that when SH decomposition is applied to decompose a directivity function measured at a distance then the directivity is considered to be free from the contribution of the near-field components (4, 5). Thus, the method is not accurate in the near-field.

ACKNOWLEDGMENTS

The research leading to these results has received funding from the People Programme (Marie Curie Actions) of the European Union's Seventh Framework Programme FP7/2007-2013 under REA grant agreement n° 290110, SONORUS "Urban Sound Planner".

REFERENCES

1. Vigeant, M. C. Investigations of incorporating source directivity into room acoustics computer models to improve auralizations. Ph.D. Thesis; Architectural Engineering Program, University of Nebraska- Lincoln, Nebraska, USA 2008.
2. Escolano, J., López, J.J. & Pueo, B. Directive sources in acoustic discrete-time domain simulations based on directivity diagrams. The Journal of the Acoustical Society of America 2007; 121(6):256-262.
3. Escolano, J., López, J.J. & Pueo, B. Broadband directive sources for acoustic discrete-time simulations. The Journal of the Acoustical Society of America 2009; 126(6):2856-59.
4. Hacihabiboğlu, H., Günel, B. & Ahmet, M. K.. Source directivity simulation in digital waveguide mesh-based room acoustics models. In: Audio Engineering Society 30th Conference; 15-17 March 2007; Saariselkä, Finland 2007.
5. Hacihabiboğlu, H., Günel, B. & Ahmet, M. K. (2008). Time-domain simulation of directive sources in 3-D digital waveguide mesh-based acoustical models. IEEE transactions on audio, speech, and language processing 2008; 16(5): 934-946.

6. Sakamoto, S. & Kano Y. Treatment of directive sound source for the finite-difference time-domain computation. In: Forum Acusticum 2011 ; 26 June-01 July 2011; Aalborg, Denmark 2011. p. 247-252.
7. Sakamoto, S. & Takahashi, R. Directional sound source modeling by using spherical harmonic functions for finite-difference time-domain analysis. In: ICA 2013; 02-07 June 2013; Montreal, Canada 2013.
8. Southern, A. & Murphy, D. Low complexity directional sound sources for finite difference time-domain room acoustic models. In: Audio Engineering Society 126th Convention; 07-10 May 2009; Munich, Germany 2009.
9. Vecherin, S.N., Wilson, D.K. & Ostashev, V. E. Incorporating source directionality into outdoor sound propagation calculations. The Journal of the Acoustical Society of America 2011; 130(6):3608-22.
10. Wilson, D.K., Vecherin, S.N. & Ostashev, V. E. Modeling sound fields from directive noise sources in the presence of atmospheric refraction and ground effects. In: INTER-NOISE 2012; 19-22 August 2012; New York, USA 2012.
11. Välimäki, V., Parker, J. D., Savioja, L., Smith, J.O. & Abel, J.S. Fifty years of artificial reverberation. IEEE Trans. Audio Speech Lang. Process. 2012; 20(5):1421-48.
12. Hornikx, M. Numerical modeling of sound propagation to closed urban courtyards. Ph.D. Thesis; Department of Civil and Environmental Engineering, Chalmers University of Technology, Gothenburg, Sweden 2009.
13. Hestaven J.S., Gottlieb S. & Gottlieb D. Spectral methods for time-depended problems. Cambridge monographs on applied computational mathematics; Cambridge University press 2007.
14. Hornikx, M., Waxler, R. & Forsén, J. The extended Fourier pseudospectral time-domain method for atmospheric sound propagation. The Journal of the Acoustical Society of America 2010; 128(4):1632-46.
15. Hornikx, M., De Roeck, W. & Desmet, W. A multi-domain Fourier pseudospectral time-domain method for the linearized Euler equations. Journal of Computational Physics 2012; 231(14): 4759-74.
16. Bogey, C. & Bailly, C. A family of low dispersive and low dissipative explicit schemes for flow and noise computations. Journal of Computational Physics 2004; 194(1):194-214.
17. Williams E.G. Fourier acoustics: Sound radiation and near field acoustical holography. Academic press 1999.
18. Zotkin, D.N., Duraiswami R. & Gumerov N.A. Regularized HRTF fitting using spherical harmonics. In: 2009 IEEE Workshop on Applications of Signal Processing to Audio and Acoustic; 18-21 October 2009; New York, USA 2009; p. 257-260.
19. MATLAB Release R2014b. The MathWorks, Inc.; Natick, Massachusetts, United States.
20. Schärer, Z., & Lindau, A. Evaluation of Equalization Methods for Binaural Signals. In: Audio Engineering Society 126th Convention; 07-10 May 2009; Munich, Germany 2009.
21. Mourjopoulos, J., Clarkson, P. M., & Hammond, J. K. A comparative study of least-squares and homomorphic techniques for the inversion of mixed phase signals. In: 1982 IEEE Int. Conference on ASSP; Paris, France 1982; p. 1858-61.